An implementation-focused bio/algorithmic workflow for synthetic biology

Angel Goñi-Moreno†, Marta Carcajona†, Juhyun Kim†, Esteban Martínez-García†, Martyn Amos‡ and Víctor de Lorenzo*†

† Systems Biology Program, Centro Nacional de Biotecnología, Cantoblanco-Madrid, Spain.
‡ Informatics Research Centre, Manchester Metropolitan University, United Kingdom.

E-mail: vdlorenzo@cnb.csic.es
*To whom correspondence should be addressed

Abstract

As synthetic biology moves away from trial and error and embraces more formal processes, workflows have emerged that cover the roadmap from conceptualization of a genetic device to its construction and measurement. This latter aspect (i.e. characterization and measurement of synthetic genetic constructs) has received relatively little attention thus far, but it is crucial for their outcome. An end-to-end use case for engineering a simple synthetic device is presented which is supported by information standards and computational methods, and which focuses on such characterization/measurement. This workflow captures the main stages of genetic device design and description and offers standardized tools for both population-based measurement and single-cell analysis. To this end, three separate aspects are addressed. First, the specific *vector features*. Although device/circuit design has been successfully automated, important structural information is usually overlooked, as is the case of plasmid vectors. The use of the Standard European Vector Architecture (SEVA) is advocated for selecting the optimal carrier of a design and its thorough description, in order to unequivocally correlate digital definitions and molecular devices. A digital version of this plasmid format was developed with the Synthetic Biology Open Language (SBOL) along with a software tool that allows users to embed genetic parts in vector

cargoes. This enables annotation of a mathematical model of the device's kinetic reactions formatted with the Systems Biology Markup Language (SBML). From that point onwards the experimental results and their *in silico* counterparts proceed alongside, with constant feedback to preserve consistency between them. A second aspect involves a framework for the *calibration* of fluorescence-based measurements. One of the most challenging endeavors in standardization, metrology, is tackled by reinterpreting the experimental output in light of simulation results, allowing us to turn arbitrary fluorescent units into relative measurements. Finally, integration of single-cell methods into a framework for *multicellular* simulation and measurement is addressed, allowing standardized inspection of the interplay between the carrier chassis and the culture conditions.

Introduction

Synthetic biology is concerned with the rational design and construction of biological information-processing devices[1]. The rigorous application of *engineering principles and processes* is fundamental to the success of this endeavor[2,3,4]. Significant attention is now being paid to the development of standardized *workflows*[5,6] which describe sequences of biological and algorithmic processes required to obtain a desired outcome. Such workflows specify a *tool-chain* for synthetic biology. The anticipated benefits of using them include *modularity* (allowing individual processes to be implemented in several different ways), *robustness* and *scalability*.

One of the over-arching challenges for the field is the end-to-end *automation* of biodesign[7,8] a process that includes two main stages[6]: [i] the automatic selection and/or construction of biological components, and their assembly into a network that, in principle, performs information processing according to a high-level specification, and [ii] the fine-tuning of the system components and/or architecture to obtain the desired performance. The first part of this process concerns the detailed *specification* of the components to be used[9,10] (or fabricated[11,12,13]), the attendant data representation and storage issues[14] and the correct arrangement of components into a *device/circuit* that can implement a given (logical) function. A wealth of so-called *bio-CAD* tools now exist for this latter task[15,16] e.g. SBROME[17,18] TinkerCell[19], SynBioSS[20] and CELLO[21]. In terms of *fine-tuning* (the second stage), recent developments use post-assembly modification

of constructs based on observed network behaviour[6] or the evolution of cell models[22] facilitating an iterative *homing-in* approach towards genetic designs.

The work presented in this article focuses on the latter stages of the device/circuit engineering process (that is, the implementation stages that follow the *initial* development of a given design). The specific issues addressed with the workflow discussed below include the formalization of device description regarding the sequences of the parts of the system to be constructed and the effect of plasmid vectors on performance. An early technical standard for the description of biological parts was the BioBrick[23,24], which is appropriate for the assembly of DNA segments. However, a key consideration (which is virtually neglected by earlier standards) is the variety of *plasmid vectors* that are available for the deployment of biological devices. In reality, the choice of plasmid vector can dramatically affect the performance of a given device; plasmid features such as replication origin, selection markers and expression system need to be carefully selected[25]. Finally, the correlation of experimental observations *vs.* simulation results is addressed: As computational tools to aid biodesign become more commonplace, more uniform types of circuits are reported in the literature. However, once they are built, the process of *measuring* the behavior of the designed system (in order to assess its fidelity to the desired output) may still vary substantially. This is because few existing workflows consider measurement, and teams are free to choose their own tools for this mission. Mathematical and computational modeling have become fundamental tools in synthetic biology, but they are only effective when combined with useful *in vivo* observations of synthetic systems. In this context, the workflow reported below, describes a methodology for easily mapping simulation results onto laboratory measurements.

Results and discussion

Figure 1 shows the different stages of the workflow discussed in this article. By adopting a combined experimental *in vitro* / *in silico* approach, the two perspectives become tightly coupled at key points. The various stages are ordered along time, from left to right, and they begin once a device design is established. Note that issues of design were not considered, and instead the workflow focuses on implementation and measurement. The first stage in the workflow is *Description*, in which the design of the desired construct is captured by some representation(s).

This then feeds into the *Implementation* stage, in which the construct is built (or modeled). Once the device has been implemented, *Population-level measurement* is carried out in order to obtain aggregate performance metrics. This then feeds into a *second Implementation* phase, which facilitates closer (single-cell) observations. These workflow stages are detailed as follows.

Description

In order to obtain reliable and robust performance of the device, it is of essence having control over the vector and being able to compare its performance with the same plasmid in multiple scenarios. In order to achieve this for the *in vivo* component the Standard European Vector Architecture (SEVA)[26] was adopted. This is an active[27,28,29,30] standard for the physical assembly of plasmid vectors and their nomenclature, as well as an online database of functional sequences and constructs available to the community. Along with the SEVA depiction of the *plasmid* there is a digital representation of the *device/circuit* for the *in silico* component of the workflow, for which the Synthetic Biology Open Language (SBOL)[31] is used. This provides a *standard exchange format* for synthetic biology designs (between research groups, and between different toolkits).

Implementation

In the first *in vitro* Implementation phase, the vector is assembled using standard Molecular Biology procedures. This results in the synthesis of DNA segments, which are then inserted into the carrier plasmid. In parallel with this process (i.e., during the *in silico* implementation phase), a standardized digital description using SBOL is constructed, with one SBOL document per genetic construct (Supplementary File S2). These documents are then combined (using a Java-based tool; Supplementary Tool S1), resulting in a single SBOL file containing the sequences of interest in the correct cargo position according to the restriction enzyme sequences. This tool identifies those SBOL components that are common across components (i.e., the restriction sites) and replaces all the information that exists in the cargo section from restriction site to restriction site with the functional cassette of interest. After this step, both the plasmid containing the device and its representation are fully standardized. Note that the cassette to be inserted into the cargo

section may be assembled (using any *wet* technique) or synthesized; the restriction sites of the SEVA vectors can be used in this Implementation stage or in possible post-measurement debugging.

Measurements

The use of mathematical modeling and computational analysis has become a fundamental part of synthetic biology, due to the information they provide concerning the mechanical behavior of the systems. However, this potential can only be used effectively when combined with direct *in vivo* measurements[32]. This is helped by ongoing advances in metrology (see, for instance, the TASBE tools at https://synbiotools.bbn.com). Recently, attempts have been made to standardize e.g. Relative Promoter Units (RPU)[33] as a measuring standard for promoter activity based on a comparison against a reference promoter. On a more abstract level, the Polymerase Operations Per Second (PoPs) measure[9] is abstracted as the signal carrier in transcriptional devices. However, none of these methods are free of controversy[15].

In order to simulate the model constructed in the Implementation phase, the iBioSim[34] tool was used. Conveniently, iBioSim exports reactions to a single Systems Biology Markup Language (SBML)[35] file (Supplementary File S3), which is a computational standard for the representation of biochemical networks. Importantly, this allows linking up the SBML *biochemical model* of the device with the SBOL description of its DNA components, using the methodology described by Roehner and Myers[36] (Supplementary File S4). In turn, this connects (via SBOL) with the SEVA description of the vector, giving seamless integration of information across different standards that are used for different levels of description. An additional application was developed (Supplementary Tool S2, based on libSBML[37]) for converting a given SBML file into Python coded scripts, used for for deterministic and stochastic simulations (Supplementary File S5). Importantly, the SBML model details (i.e., rates) correspond not only to the device itself, but also its carrier vector. This significantly reduces output variability: by including details of the vector in the model characterization (via SEVA/SBML), the possibility that the carrier plasmid might later change due to decisions taken at the implementation phase is considered. Any such change will, in turn, inevitably (although, sometimes subtly) affect the observable behavior of the model

when implemented. Including details of the vector thus allows to ponder fluctuations due to variable plasmid selection.

The inclusion of an extra step within the workflow for *multicellular* analysis also helps reducing the variability caused by both the chassis and the culture conditions, as they add their own effects to the construct and its carrier. If the device has to be used under different scenarios, the cellular behavior should be quantified. There are behaviors in the example provided, that cannot be measured with the cytometer (i.e., noise inheritance or cell movement), and which require time-lapse microscopy in order to be quantified. The parameters corresponding to these behaviors are therefore fitted according to single-cell measurements. Again, this information adds value to a potential specification sheet that accompanies the *in vivo* system.

Spectophotometry is used to measure the fluorescent signal of the entire cell population; dividing this by the optical density at 600 nm (OD_{600}) over time yields the average fluorescence value per cell in the culture. Experimental values are used to fit kinetic rate parameters in the mathematical models so they produce similar profiles. Importantly, in the graphs that follow, the Y-axis refers to *arbitrary units* of fluorescence in experimental observations, and the *number of molecules* (for example, mCherry proteins) in the simulated observations. Matching the latter with the former gives an important reference point concerning measurements, which allows interpretation of subsequent results.

Stochastic analyses are then done in order to characterize noise in the system, using the well established Gillespie algorithm[38]. On the experimental front, data on noise is obtained using flow cytometry, which allows user to check the fluorescence intensity value of (in principle) every single cell in the bacterial culture. Although the ready-to-use graphs produced by the cytometer (Supplementary Figure S1) are used as standard in most laboratories, *raw values* were preferred before they are processed for presentation (normally in a *black box* fashion, which is opaque to the user). There are three main reasons for using raw cytometry data: [i] Cytometers *count* cells using variable intervals of fluorescence at high values of a logarithmic scale that is not always constant, and which depends on a specific machine set-up. This processing therefore introduces variability that is hidden from the user; [ii] cell-specific values are needed in order to make direct

comparisons with simulated cells within our framework; (3) raw data values are more amenable to importing and processing by various tool-chain components. In contrast, automated extraction of specific values from graphs produced by cytometers introduces unnecessary complications and the possibility of misreading data.

A simulated cytometry graph is obtained by running the Python version of the reactions (see Methods). This offers two potential benefits. On one hand, it gives a computational method (*via* an SBML model) of discarding invalid values from the raw cytometry information (see the later Case study for an example). On the other hand, by overlapping both experimental and simulated plots the arbitrary units (*au*) of the cytometer and those from the spectrophotometer could be correlated. This procedure seems therefore to help unifying machine-based measurements in the Laboratory, as shown in the case study below.

Implementation

The behavior of the device under study is inevitably affected by the specific attributes of the host cell. A thorough characterization of a construct should, therefore, include information about the performance of the *chassis*[39] (which, in the case shown, is *E.coli* CC118[40]). Rather than simply providing *added value,* this information is of vital importance in the case of multicellular applications[41,42], which are becoming increasingly important as cell-to-cell communications are increasingly well-understood and customised[43,44].

In order to study the behavior of devices *in vivo* the DiSCUS[4] package previously developed to study bacterial growth was adopted as an agent-based simulation tool. Importantly, this platform considers *physical forces* between rod-shaped bacteria and is applicable to a wide range of organisms. DiSCUS uses the previously generated Python scripts for the intra-cellular genetic network that is implemented in the cells of interest. The SBML model is therefore embedded into the cellular objects of the agent-based simulator. Note that there is a standard, currently under development, called the Multi-Cellular Data Standard (MultiCellDS, http://multicellds.org/), which aims at sharing multicellular experimental, simulation and clinical data. Hopefully, when released, it will facilitate partaking of configuration parameters for a specific chassis performance.

In the case under examination (see below), a 2-dimensional culture was prepared on an agarose pad[46], and the cells let to grow on a monolayer in order to facilitate visualization in the microscope.

Single-cell measurements

The movement and the growth of the simulated cells were first calibrated according to experimental observations. For this, the successive positions of a specific cell until division were monitored and the displacement of its offspring during their lifetime(s) followed. These results were matched against the equivalent information obtained from the simulations, and adjusted to DiSCUS parameters for fitting the experiments. In short (see Methods for more details), this information yields the most relevant features to prioritize in DiSCUS in order to reproduce the movement of the cells *in vivo* (see example below).

Spatial measurements

After characterizing the dynamics of the chassis that host the construct, its performance in a spatial scenario was measured. For this, we quantified the fluorescence intensity of the device *in vivo*, and obtained a pixel-based image analysis of the specific color (red in the example,) captured by the microscope. The ensuing analysis translates the scale bar into values proportional to those used in the mathematical model (see Methods for details of this conversion). As a consequence, a simulation run with the system's equations inside DiSCUS bodies, could be directly compared with experiments in respect to device function.

Case study

A combined *in vivo/in silico* study involving a simple construct was picked as an informative example of the proposed workflow. The starting point was an *always-on* gene expression device i.e. a genetic module enabling constitutive transcription and translation of a reporter gene (mCherry; Figure 2A). Although this setup involves just a few components, it was also instrumental to highlight the main focus of this work, which lies on the *measurement* of such devices. That is, the complexity of the device to be constructed is less critical than the

management of its *output*. Given that fluorescence measurements are taken in fundamentally in the same way, regardless of the size or complexity of a synthetic device, the question at stake is how such metrics might be *standardized*, and relate them back to *in silico* studies in a useful and meaningful way.

As shown in Figure 2A the two subcomponents of the device were [i] the pEM7 constitutive promoter, and [ii] the red fluorescence reporter gene *mCherry* (see Methods for details; Supplementary File S1). Once the initial design was in place the system was taken to the Description stage, where *pEM7-mCherry* was digitally formalized and physically built. The pSEVA231 vector (Figure 2B) was selected to implement the design. This plasmid contains a kanamycin marker, an origin of replication pBBR1, and the default cargo segment. As the cargo segment is a sequence of restriction sites, specific locations have to be selected for inserting the desired parts. As shown in Figure 2A, the promoter component was flanked by restriction sites PacI and AvrII, while HindIII and SpeI were chosen for the reporter gene –thereby leaving a number of *empty* sites in between for a possible future usage.

Once the Description phase was complete, the system was taken to the Implementation stage. Figure 3A highlights the kinetic rates involved and the Ordinary Differential Equations (ODEs) that govern the continuous functioning of the *always-on* device. After cloning, Figure 4A shows the results for average fluorescence value per cell in the culture, along with deterministic simulation runs (based on the ODEs) for both the SBML model (implemented using iBioSim) and its corresponding Python script. The stage was thus set to move to the Population measurement phase.

Figure 4B shows the fluctuations in molecular levels of the reactions of Figure 3A when running the Gillespie algorithm on the SBML model (iBioSim) and its corresponding Python file. As expected, the observed variability was the same in both, as the kinetic rates remain unchanged (i.e., the same as in the ODEs). The mean value was precisely situated on the steady state value of the deterministic simulation. Raw data from the cytometer are plotted on Figure 4C, where the bimodal curve indicates that approximately half of the cells displayed a strong fluorescence,

while the rest expressed none (or very little). The latter group corresponded to invalid values, and could be discarded, as indicated by the control data (the same strain without the plasmid) and the already processed graph (Supplementary Figure S1). Moreover, further microscopy tests showed strong fluorescence in all the cells with a relatively narrow noise interval, which confirms the correct elimination of that non-expressing cell group. As described in the workflow description, this gives a computational standard way of discarding invalid values from raw cytometry information. Moreover, it yields a method for correlating outputs from different pieces of laboratory equipment. We illustrate this in the graph of Figure 4C, showing that Arbitrary Units (*au*) of the cytometer could be correlated with those from the spectrophotometer: 1 *au* in the former, and $\simeq$ 1.2 *au* in the latter (see Methods for details).

After performing population-level measurements, the workflow proceeds to single-cell measurements. Figure 5A shows the result of experiments to track cell movements. Figure 5B shows the positions of a bacterium (from Figure 5A) until division, and then the displacement of its daughter cells during their lifetime. Figure 5C shows the most relevant features needed for adding to DiSCUS in order to reproduce the movement of the bacteria, starting from a very simple growth algorithm (which returns unrealistic patterns; Figure 5C.1). Ultimately, the qualities to be considered include [i] *cell size variations* (due to conditional growth), [ii] changes in *transversal angles* after division, [ii] *randomised directions of movement*, and [iv] slight *attraction between cells* (in order to avoid the appearance of holes within the colony).

Figure 5D compares the synchrony of growth within experimental and simulated cells, yielding suggestions as to how to uncouple growth events. These graphs show the length of each cell in the population over *time* (in Laboratory experiments) or *iterations* (in the simulation). Starting with just two cells (the same setup as in Figure 5A) that grow and divide at the same time it becomes apparent that the length of the cells is no longer synchronized after the second division (eight cells in total).

The spatial scenario is considered next. Figure 6A shows the results of measuring the fluorescence intensity of the *pEM7-mCherry* device when placed in the *E. coli* CC118 strain along with a pixel-based image analysis of the red color captured by the microscope. As indicated

above, the scale bar of the analysis was translated into values proportional to those of the mathematical model of Figure 4B. A simulation run in DiSCUS, using the system's equations (Figure 6B, left) can be directly compared against experiments. For instance, its it possible to verify that daughter cells share output levels as they directly *copy* their mother's device at a given time (Figure 6B). Also, that cells with slower growth tend to display a stronger light signal (due to the accumulation of fluorescence proteins).

Conclusion

Development of standardized workflows that allow for robust and reproducible genetic constructs is one of the contemporary challenges of synthetic biology. The frame presented above contributes to this endeavor by setting both computational and experimental approaches to build and measure synthetic devices, using a simple synthetic device as an example. This approach is different and complementary of other efforts that focus on specific steps e.g. automated circuit design[5,16,18], mathematical modelling[20], single-cell analysis[46], metrology[33], data representation[31] or post-construction modification[6]. In contrast the workflow presented in this article can make use of several of them by concentrating on output measurements, what is ideal for design-oriented efforts. While the literature records other workflow propositions[15], they tend to focus on enumeration rather than application of techniques. Instead, the tools presented here allow linking standards, e.g. merging SBOL documents for SEVA description, or the scripts to translate SBML into Python. The system will hopefully provide a useful starting point for newcomers to the field, as well as (more generally) a standard workflow for robust programming of biological systems.

Materials and Methods

Strains and plasmids. The *E. coli* strain used in this work was CC118[40]. The vector plasmid for the expression device was pSEVA231 (kanamycin resistance, pBBR1 origin of replication and default SEVA cargo) selected from the database http://seva.cnb.csic.es/. pEM7 promoter was cloned in pSEVA231 as a PacI/AvrII fragment and the mCherry reporter gene as a HindIII/SpeI DNA segment. The resulting plasmid was named pSEVA237R-pEM7 (available in the SEVA

database). An important aspect is that sequences of interest encoding the expression device were edited to remove any restriction site incompatible with the SEVA standard.

SBOL-SEVA description. The SEVA format is highly structured in unambiguous functional segments, as shown in Figure 2B. The SEVA vector 231 was described using SBOL-2.0[47,48], (Supplementary Figure S2). The previous description of this vector using the GenBank format[49] was improved by adding missing features (e.g. assembly scars), and by establishing structural and functional links. Two more SBOL documents were produced, one for each component of the device. Ultimately, a Java based application was developed that could be fed with the carrier plasmid and the cassettes that need to be inserted, and outputs the composite vector. The application searches in the carrier file for those restriction sites present in the cassettes (iteratively) and replaces the sequence in between. The resulting SBOL document has all location parameters (i.e. *bioStart*) updated.

Mathematical modelling and SBML-to-Python conversion. In the model of Figure 3A, we show the promoter-reporter pair (18 copies, as estimated by previous observations for pBBR1 origin of replication[50]), *mRNA* the messenger RNA and *rfp,* the red fluorescent protein (both at 0 molecules at the beginning of the simulation). Regarding the kinetic rates: k_1 is the transcription rate (27/18 $hour^{-1}$ from each plasmid), k_2 represents the translation rate (2.5 $hour^{-1}$), k_3 the degradation rates of the mRNA (0.65 $hour^{-1}$) and k_4 the protein degradation rates (0.265 $hour^{-1}$). Note that for such a small network, parameter assignment is non-trivial due to the number of constraints. The effort for assigning numbers to rates[51] is thus of vital importance at this stage. The software iBioSim (http://www.async.ece.utah.edu/iBioSim/) was then used to write the model in SBML format and run the simulations with the Hierarchical Runge-Kutta method for ODEs solution, along with the Gillespie algorithm for stochastic behavior. The model was exported in a *flat* (iBioSim option) XML file and converted into Python scripts with the tool provided (Supplementary Tool S2). Flow cytometry data was obtained from the FCS files without processing, and the simulated graph was obtained by [i] sampling a stochastic run in time (forcing equal time intervals), [ii] counting intensity values over a long enough (~ 600 hours) period and [iii] reinterpreting x-axis values (originally, time) as individual cells in order to

represent an intensity distribution comparable to the experimental plots. By making the simulations match experiments (Figure 4A), its appeared that ~ 400 simulated molecules (s.m.) corresponded to ~ 400 arbitrary units in the spectrophotometer (a.u.s). As the computational measurements (s.m.) in the stochastic simulation are exactly the same, they were correlated with the fluorescent units of the cytometer (a.u.c). As Figure 4C shows, ~ 400 s.m. = ~ 330 a.u.c; therefore 1 a.u.s = 400/330 a.u.c. We assume that the sources of fluorescent signal are the same, as the cells remained unaltered.

Two-dimensional *in-vivo* setup. Samples for the microscope were prepared with agarose pads on a slide glass with an attached frame (1.7 X 2.8 cm, Life Technologies) following the method described by de Jong *et al.*[52] To this end, 500 µl of LB, including 2% of melted agarose was added into the middle of the frame and assembled with another slide glass. After 30 min at room temperature, one of the slide glasses was carefully removed, maintaining an intact agarose pad. Then, the pad was cut out to 5 mm width within the frame using a razor blade and two strips of the pad used for supporting growth of the bacterial cells. For this, strain carrying pSEVA237R-pEM7 was pre-cultured overnight in LB at 37º C, diluted 100-fold in the same medium and grown to exponential phase (OD_{600} = 0.2). 2.5 µl of the samples were then spotted on to the agarose pad and assembled with cover glasses (24 x 50 mm) for further analysis. Widefield fluorescent microscopy was used to observe the samples (Leica DMI6000B, Leica Microsystems) with a digital CCD camera Orca-R2 (Hamamatsu). Cell growth was monitored for 75 min under the microscope at 37º C and images were captured every 3 min with a40.0x/0.75 NA dry objective or a 63.0x/1.3 NA glycerol immersion objective (depending on the experiment) with a bandpass filter for mCherry (BP 560/40 and EM 645/75.) using the LAS AF v. 2.6.0 software (Leica Microsystems). Images were analyzed with the MATLAB-based code Schnitzcells[53] in order to track both the positions of the cells and their length while growing.

Two-dimensional *in-silico* setup. DiSCUS (http://code.google.com/p/discus/) is an agent-based

354 software for bacterial growth that uses Pymunk (http://pymunk.readthedocs.org/en/latest/), a 2D
355 physics library, to resolve collisions among cells. In the most basic test of Figure 5C.1 each cell
356 is a body of 16x30 square lattice that grows lengthwise until division, when the cell is cut in half.
357 Pressure-based growth is simulated by counting the cells that push a body of interest (threshold at
358 4 cells) and slowing down the growth events (without stopping them). Random angle variations
359 were introduced after division, whereby the daughter cells *copy* the angle of the mother and add a
360 number in the interval (-25,25) degrees. Furthermore, angle variations were included at the
361 normal growth events, although to a smaller extent (maximum variation of 5 degrees). The fact
362 that the cells grow *in vivo* forming a circular group without holes was simulated using a slight
363 gravity-like value that pushed the cells towards the middle of the population. This force can be
364 eliminated when the population is about 20 cells big, at which point the circular shape is
365 conserved without any other attraction.

366 Regarding pixel intensity in the analysis of Figure 6A, the maximum value was set to be at the
367 same level as the highest peak of the stochastic simulation of Figure 4B or the cytometry data of
368 Figure 4C (~ 470 a.u.). Therefore we calculated the percentage rate (470 times 100 divided by the
369 maximum pixel value) to convert the intensity of every pixel into the scale shown by experiments.
370 Again, we assume that the source of light is the same (*E.coli* CC118) and variances are due to
371 different machine measurements.

372 # Acknowledgement

373 This work was supported by the CAMBIOS Project of the Spanish Ministry of Economy and
374 Competitiveness, the EVOPROG, ARISYS and EMPOWERPUTIDA contracts from the
375 European Union, and the PROMT Project of the Madrid regional government to VdL. The
376 Authors declare no conflict of interest.
377

378 # References

(1) Church, G. M.; Elowitz, M. B.; Smolke, C. D.; Voigt, C. A.; Weiss, R. (2014) Realizing the potential of Synthetic Biology. *Nat. Rev. Mol. Cell Biol.*, *15*, 289–294.

(2) Andrianantoandro, E.; Basu, S.; Karig, D. K.; Weiss, R. (2006) Synthetic biology: new engineering rules for an emerging discipline. *Mol. Syst. Biol.*, *2:1*.

(3) Heinemann, M.; Panke, S. (2006). Synthetic biology - putting engineering into biology. *Bioinformatics*, *22*, 2790–9.

(4) Kitney, R.; Freemont, P. (2012) Synthetic biology - the state of play. *FEBS Letters*, *586*, 2029–2036.

(5) Beal, J.; Weiss, R.; Densmore, D.; Adler, A.; Appleton, E.; Babb, J.; Bhatia, S.; Davidsohn, N.; Haddock, T.; Loyall, J.; Schantz, R.; Vasilev, V.; Yaman, F. (2012) An end-to-end workflow for engineering of biological networks from high-level specifications. *ACS Synth. Biol.*, *1*, 317–331.

(6) Litcofsky, K. D.; Afeyan, R. B.; Krom, R. J.; Khalil, A. S.; Collins, J. J. (2012) Iterative plug-and-play methodology for constructing and modifying synthetic gene networks. *Nat. Methods*, *9*, 1077–1080.

(7) Brophy, J. A.; Voigt, C. A. (2014) Principles of genetic circuit design. *Nat. Methods*, *11*, 508–520.

(8) Densmore, D. M.; Bhatia, S. (2014) Bio-design automation: software + biology + robots. *Trends Biotechnol.*, *32*, 111–113.

(9) Baker, D.; Church, G.; Collins, J.; Endy, D.; Jacobson, J.; Keasling, J.; Modrich, P.; Smolke, C.; Weiss, R. (2006) Engineering life: building a fab for biology. *Sci. Am.*, *294*, 44–51.

(10) Varadarajan, P. A.; Del Vecchio, D. (2009) Design and characterization of a three-terminal transcriptional device through polymerase per second. *NanoBioscience, IEEE Trans.*, *8*, 281–289.

(11) Nielsen, A. A.; Segall-Shapiro, T. H.; Voigt, C. A. (2013) Advances in genetic circuit design: novel biochemistries, deep part mining, and precision gene expression. *Curr. Opin. Chem. Biol., 17*, 878–892.

(12) Khalil, A. S.; Lu, T. K.; Bashor, C. J.; Ramirez, C. L.; Pyenson, N. C.; Joung, J. K.;

Collins, J. J. (2012) A synthetic biology framework for programming eukaryotic transcription functions. *Cell*, *150*, 647–658.

(13) Villalobos, A.; Ness, J. E.; Gustafsson, C.; Minshull, J.; Govindarajan, S. (2006) Gene Designer: a synthetic biology tool for constructing artificial DNA segments. *BMC Bioinf.*, *7*, 285.

(14) Canton, B.; Labno, A.; Endy, D. (2008) Refinement and standardization of synthetic biological parts and devices. *Nat. Biotechnol.*, *26*, 787–793.

(15) MacDonald, J. T.; Barnes, C.; Kitney, R. I.; Freemont, P. S.; Stan, G.-B. V. (2011) Computational design approaches and tools for synthetic biology. *Integr. Biol.*, *3*, 97–108.

(16) Marchisio, M. A.; Stelling, J. (2009) Computational design tools for synthetic biology. *Curr. Opin. Biotechnol.*, *20*, 479–485.

(17) Huynh, L.; Tsoukalas, A.; Köppe, M.; Tagkopoulos, I. (2013) SBROME: a scalable optimization and module matching framework for automated biosystems design. *ACS Synth. Biol.*, *2*, 263–273.

(18) Huynh, L.; Tagkopoulos, I. (2014) Optimal part and module selection for synthetic gene circuit design automation. *ACS Synth. Biol.*, *3*, 556–564.

(19) Chandran, D.; Bergmann, F. T.; Sauro, H. M. and others. (2009) TinkerCell: modular CAD tool for synthetic biology. *J. Biol. Eng.*, *3*, 19.

(20) Hill, A. D.; Tomshine, J. R.; Weeding, E. M.; Sotiropoulos, V.; Kaznessis, Y. N. (2008) SynBioSS: the synthetic biology modeling suite. *Bioinformatics*, *24*, 2551–2553.

(21) Nielsen, A. A.; Der, B. S.; Shin, J.; Vaidyanathan, P.; Paralanov, V.; Strychalski, E. A.; *et al.* (2016). Genetic circuit design automation. *Science*, 352(6281), aac7341.

(22) Cao, H.; Romero-Campero, F. J.; Heeb, S.; Cámara, M.; Krasnogor, N. (2010) Evolving cell models for systems and synthetic biology. *Syst. Synth. Biol.*, *4*, 55–84.

(23) Knight, T. (2003) *Idempotent vector design for standard assembly of biobricks*; DTIC Document.

(24) Shetty, R. P.; Endy, D.; Knight Jr, T. F. (2008) Engineering BioBrick vectors from BioBrick parts. *J. Biol. Eng.*, *2*, 1–12.

(25) Preston, A. (2003) Choosing a cloning vector. *E. coli Plasmid Vectors*; Springer, 2003; pp

19–26.

(26) Martínez-García, E.; Aparicio, T.; Goñi-Moreno, A.; Fraile, S.; de Lorenzo, V. (2014) SEVA 2.0: an update of the Standard European Vector Architecture for de-/re-construction of bacterial functionalities. *Nucleic Acids Res.*, gku1114.

(27) Calero, P.; Jensen, S. I.; Nielsen, A. T. (2016). Broad host range ProUSER vectors enable fast characterization of inducible promoters and optimization of p-coumaric acid production in Pseudomonas putida KT2440. *ACS Synth. Biol*.

(28) Wright, O.; Delmans, M.; Stan, G.-B.; Ellis, T. (2014). GeneGuard: a modular plasmid system designed for biosafety. *ACS Synth. Biol.*, 4(3), 307-316.

(29) Kim, S. H.; Cavaleiro, A. M.; Rennig, M.; Nørholm, M. H. H. (2016). SEVA linkers: a versatile and automatable DNA backbone exchange standard for synthetic biology. *ACS Synth. Biol*.

(30) Zobel, S.; Benedetti, I.; Eisenbach, L.; de Lorenzo, V.; Wierckx, N.; Blank, L. M. (2015). Tn7-Based Device for Calibrated Heterologous Gene Expression in *Pseudomonas putida. ACS Synth. Biol.*, 4(12), 1341-1351.

(31) Galdzicki, M.; Clancy, K. P.; Oberortner, E.; Pocock, M.; Quinn, J. Y.; Rodriguez, C. A.; Roehner, N.; Wilson, M. L.; Adam, L.; Anderson, J. C. and others (2014) The Synthetic Biology Open Language (SBOL) provides a community standard for communicating designs in synthetic biology. *Nature Biotechnol.*, *32*, 545–550.

(32) Kelwick, R.; MacDonald, J. T.; Webb, A. J.; Freemont, P. (2014) Developments in the tools and methodologies of synthetic biology. *Front. Bioeng. Biotechnol.*, *2*.

(33) Kelly, J. R.; Rubin, A. J.; Davis, J. H.; Ajo-Franklin, C. M.; Cumbers, J.; Czar, M. J.; de Mora, K.; Glieberman, A. L.; Monie, D. D.; Endy, D. (2009) Measuring the activity of BioBrick promoters using an in vivo reference standard. *J. Biol. Eng.*, *3*, 4.

(34) Myers, C. J.; Barker, N.; Jones, K.; Kuwahara, H.; Madsen, C.; Nguyen, N.-P. D. (2009) iBioSim: a tool for the analysis and design of genetic circuits. *Bioinformatics*, *25*, 2848–2849.

(35) Hucka, M.; Finney, A.; Sauro, H. M.; Bolouri, H.; Doyle, J. C.; Kitano, H.; Arkin, A. P.; Bornstein, B. J.; Bray, D.; Cornish-Bowden, A. and others. (2003) The systems biology

markup language (SBML): a medium for representation and exchange of biochemical network models. *Bioinformatics*, *19*, 524–531.

(36) Roehner, N.; Myers, C. J. (2013) A methodology to annotate systems biology markup language models with the synthetic biology open language. *ACS Synth. Biol. 3*, 57–66.

(37) Bornstein, B. J.; Keating, S. M.; Jouraku, A.; Hucka, M. (2008) LibSBML: an API library for SBML *Bioinformatics*, *24*, 880–881.

(38) Gillespie, D. T. (1976) A general method for numerically simulating the stochastic time evolution of coupled chemical reactions. *Journal of Computational Physics 22*, 403–434.

(39) Danchin, A. (2012) Scaling up synthetic biology: do not forget the chassis. *FEBS Letters 586*, 2129–2137.

(40) Manoil, C.; Beckwith, J. (1985) TnphoA: a transposon probe for protein export signals. *Proc. Natl. Acad. Sci.*, 82(23), 8129-8133.

(41) Amos, M. (2014) Population-based microbial computing: a third wave of synthetic biology?. *Int. J. Gen. Syst. 43*, 770–782.

(42) Macía, J.; Posas, F.; Solé, R. V. (2012) Distributed computation: the new wave of synthetic biology devices. *Trends Biotechnol. 30*, 342–9.

(43) Tamsir, A.; Tabor, J. J.; Voigt, C. A. Robust multicellular computing using genetically encoded NOR gates and chemical 'wires'. *Nature 469*, 212–5.

(44) Goñi-Moreno, A.; Amos, M.; de la Cruz, F. (2013) Multicellular computing using conjugation for wiring. *PLOS ONE 8*, e65986.

(45) Goni-Moreno, A.; Amos, M. (2015) DiSCUS: A simulation platform for conjugation computing. *Unconventional and Natural Computation* (UCNC 2015), Auckland, New Zealand, August 31-September 4, 2015.

(46) Skinner,S.O.; Sepúlveda, L. A.; Xu, H.; Golding, I. (2013) Measuring mRNA copy number in individual Escherichia coli cells using single-molecule fluorescent in situ hybridization. *Nat. Protoc. 8*, 1100–1113.

(47) Bartley, B.; Beal, J.; Clancy, K.; Misirli, G.; Roehner, N.; Oberortner, E.; *et al.* (2015). Synthetic Biology Open Language (SBOL) Version 2.0. 0. *J. Int. Bioinformatics*, 12, 272.

(48) Roehner, N.; Beal, J.; Clancy, K.; Bartley, B.; Misirli, G.; Gruenberg, R.; *et al.* (2016).

Sharing Structure and Function in Biological Design with SBOL 2.0. *ACS Synth. Biol.*

(49) Benson, D. A.; Karsch-Mizrachi, I.; Lipman, D. J.; Ostell, J.; Rapp, B. A.; Wheeler, D. L. (2000) GenBank. *Nucleic Acids Res. 28*, 15–18.

(50) Lee, T. S.; Krupa, R. A.; Zhang, F.; Hajimorad, M.; Holtz, W. J.; Prasad, N.; Lee, S. K.; Keasling, J. D. (2011) BglBrick vectors and datasheets: a synthetic biology platform for gene expression. *J. Biol. Eng. 5*, 1–14.

(51) Ronen, M.; Rosenberg, R.; Shraiman, B. I.; Alon, U. (2002) Assigning numbers to the arrows: parameterizing a gene regulation network by using accurate expression kinetics. *Proc. Natl. Acad. Sci. 99*, 10555–10560.

(52) de Jong, I. G.; Beilharz, K.; Kuipers, O. P.; Veening, J.-W. (2001) Live cell imaging of Bacillus subtilis and Streptococcus pneumoniae using automated time-lapse microscopy. *J. Visualized Exp.: JoVE, 53.*.

(53) Young, J. W.; Locke, J. C.; Altinok, A.; Rosenfeld, N.; Bacarian, T.; Swain, P. S.; Mjolsness, E.; Elowitz, M. B. (2012) Measuring single-cell gene expression dynamics in bacteria using fluorescence time-lapse microscopy. *Nat. Protoc. 7*, 80–88.

Supporting Information Legends

Supplementary File S1. Sequences of promoter pEM7 and gene mCherry.

Supplementary File S2. SBOL files. For a) plasmid, b) promoter and c) reporter.

Supplementary Tool S1. Software tool to merge SBOL files and insert cassettes into a vector.

Supplementary File S3. SBML files.

Supplementary File S4. Annotated SBML file.

Supplementary Tool S2. Software tool to convert a SBML model into a Python script.

Supplementary File S5. Python scripts

9 Supplementary Figure S1. Cytometry results. Graph output by cytometer after processing.

Figures

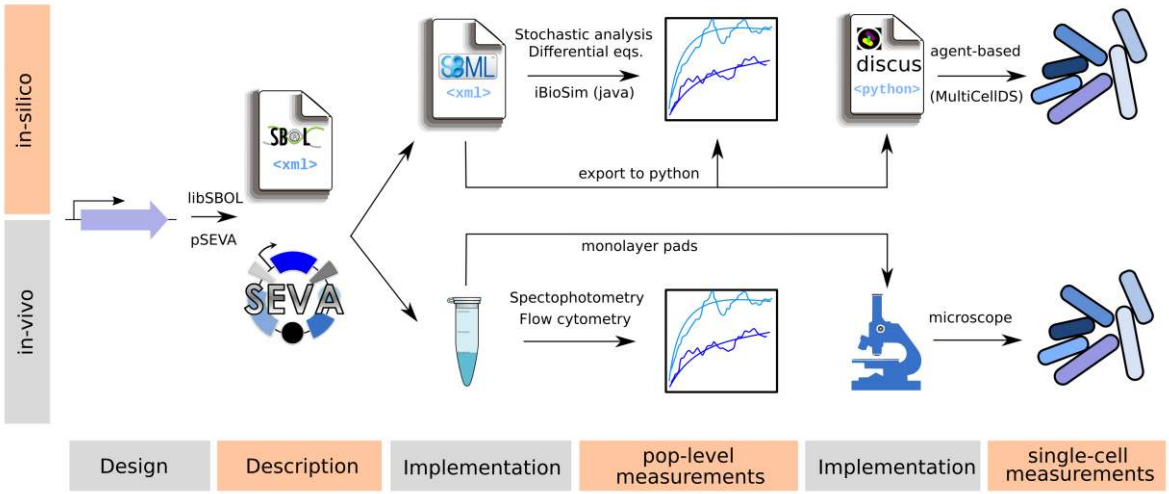

Figure 1: **Workflow for an end-to-end synthetic biology use case**. The description that follows (and modifies) the design of an idea is the starting point for the consequent experimental and computational methods. The device and its carrier vector are described using the SEVA (Standard European Vector Architecture) format for the *in vivo* workflow and the SBOL (Synthetic Biology Open Language) standard for the parallel *in silico* process. A first implementation round is then performed via synthesis and cloning methods in the wet-lab and *via* SBML (Systems Biology Markup Language) for the modeling. The resulting material is then used for different measurements. First, laboratory equipment is used for population-based experiments (spectophotometry and flow cytometry) to compare the output against simulation software (iBioSim and *ad hoc* python code). Another implementation round prepares the samples for single-cell measurements. On the computational side, the SBML model is exported to a Python script ready to be used with the software for cell movement DiSCUS (Discrete Simulation of Conjugation Using Springs). On the other side, the cells are grown on an agarose pad for 2-dimensional populations that allow matching results.

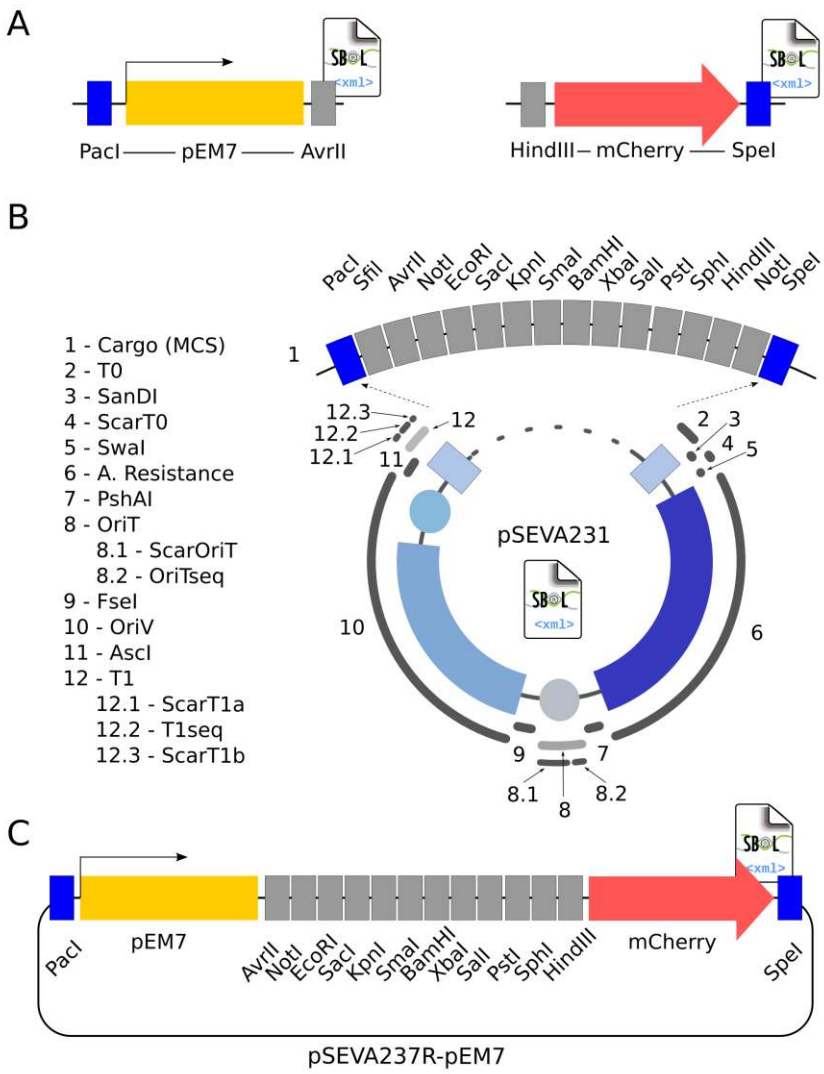

Figure 2: **SBOL description of device and SEVA components. A.** Design modification where the components are flanked by the selected restriction sites that specify their situation inside the SEVA vector. The constitutive promoter pEM7 is surrounded by PacI and AvrII sites, whereas the reporter mCherry is flanked by HindIII and SpeI. An SBOL document per component is created. **B.** The plasmid selected to harbor the device is SEVA number 231 (kanamycin resistance, pBBR1 origin of replication, default cargo). All vector features are recorded in a single SBOL document, including the cargo (multiple cloning site) component for a further assembling of device-forming parts. **C.** Both *in vivo* and *in silico* protocols for building the final construct have the same basics i.e. introducing parts sequentially in the carrier vector. A software tool (Supplementary Tool S1) allows to do so with SBOL documents.

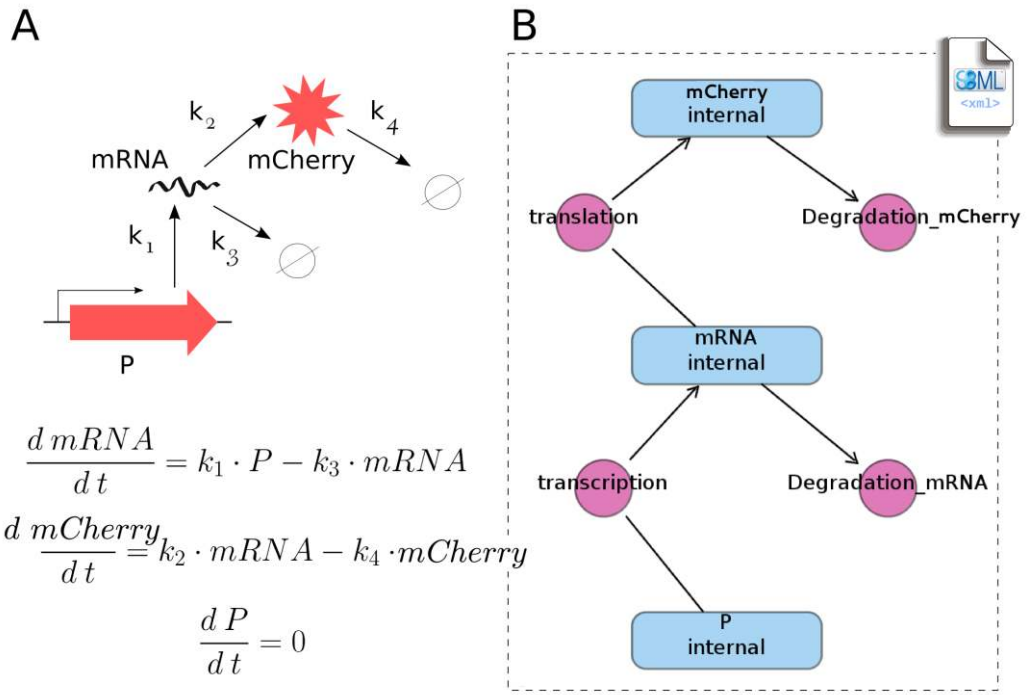

Figure 3: **Mathematical modeling and its SBML format A.** Kinetic reactions (up) and system's differential equations (bottom). The device's behavior can be effectively simulated with just four kinetic constants: the constitutive promoter *P* facilitates reporter transcription with rate k_1, resulting mRNA is translated with rate k_2 leading to the formation of RFP (red fluorescent protein) and both elements are degradated with rates k_3 and k_4 respectively. ODEs (Ordinary Differential Equations) governing continuous dynamics are shown. **B.** Scheme of the SBML model produced with the software iBioSim, a CAD (computer-aided design) package for systems biology. In the screenshot, blue elements represent substrates and red circles hide reaction rates. After setting the parameters, iBioSim allows the user to export the model to an XML file formatted following the SBML standard.

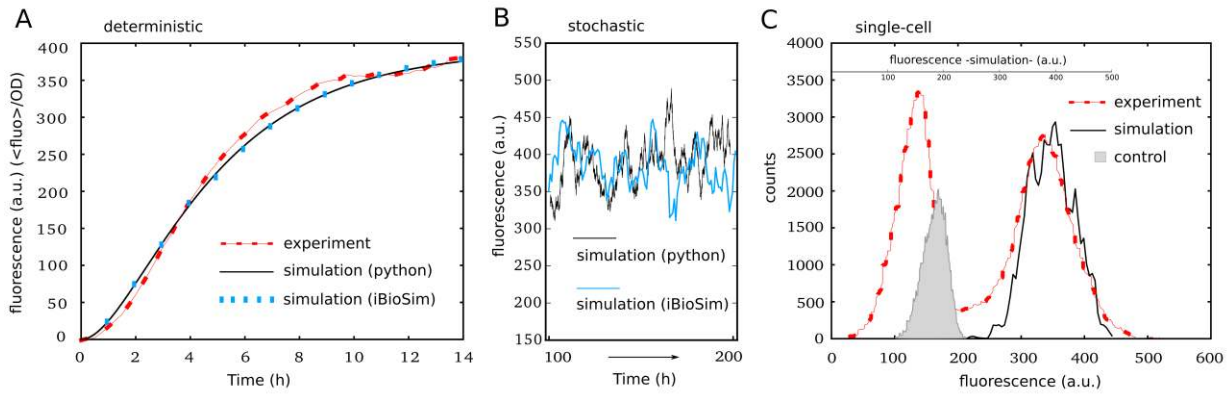

559

560 Figure 4: **Population-based measurements in experimental and simulation setups. A.**
561 Deterministic functioning of the device, in terms of fluorescence intensity over time (during 14
562 hours), averaging the value of the whole population. Red line corresponds to experimental results,
563 while blue and black lines show simulation runs of the model's differential equations with
564 iBioSim and Python code respectively. Experimental values were used to fit rate numbers in
565 mathematical models so they produce similar continuous lines. **B.** Stochastic behavior of the
566 system according to simulations. The blue line results of running the Gillespie algorithm with
567 iBioSim whereas the black line shows the python script behavior. As expected (same algorithm
568 with equal parameters), the fluctuations are alike. **C.** Fluorescence intensity values of each cell in
569 the population measures variability and expression noise. Experimental raw data extracted by
570 flow cytometry (without processing by the cytometer, see text for details) corresponds to the red
571 line. Black line results from counting expression values in the simulation with the Python script,
572 while grey area represents the control (plasmid-free cells) measured experimentally. Note that
573 scales are different in simulation and experimental lines, standing for variability within arbitrary
574 units (a.u.).

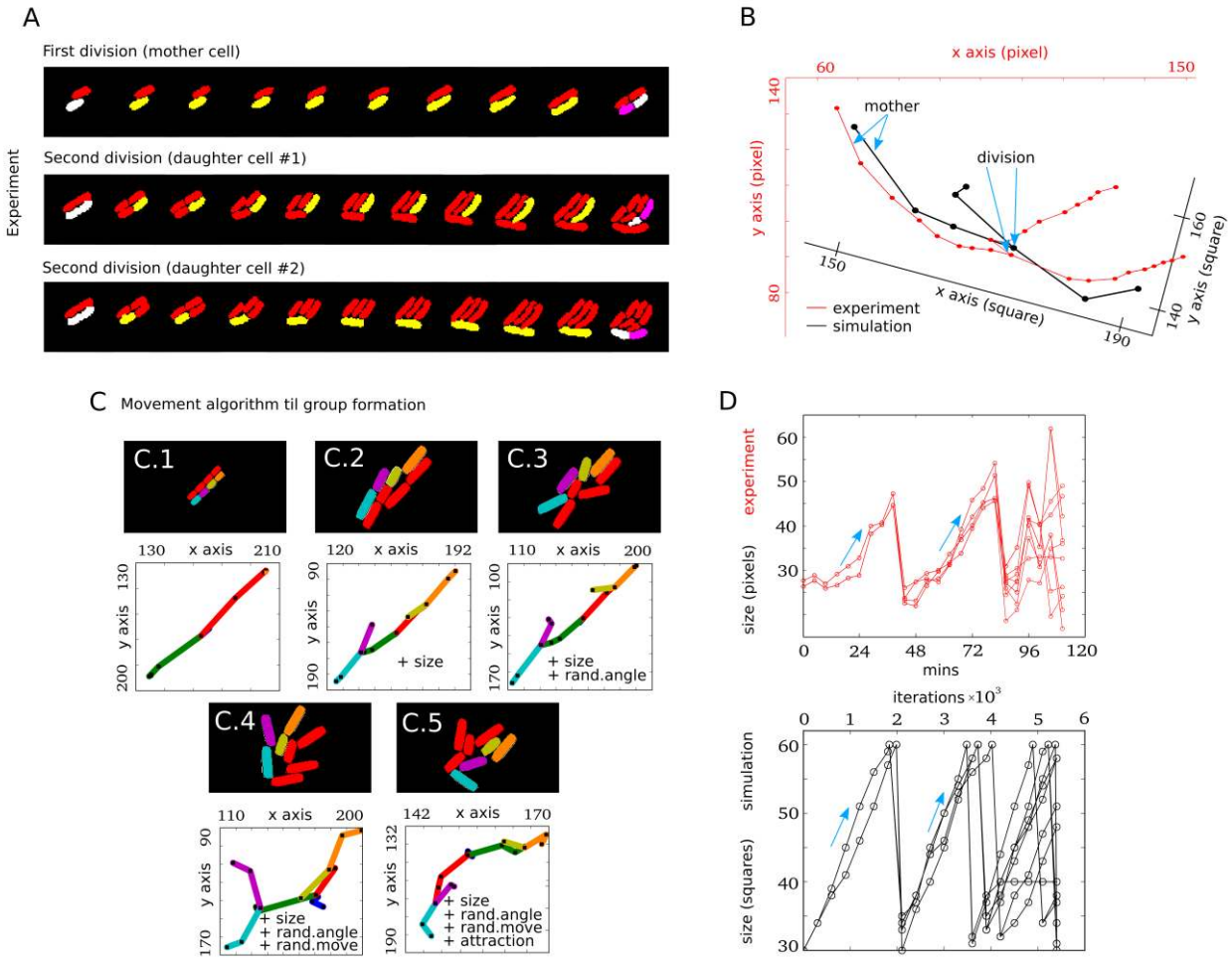

575

576 Figure 5: **Characterization of chassis mechanics. A.** Tracking cell lineages in an experimental
577 setup. Starting from the division of a single cell (up) the movement of its daughters were
578 followed (middle and bottom) in order to define their movement behavior until next division. **B.**
579 Position coordinates are recorded during the experiment (red line) and simulation (black line) to
580 fit parameters by comparing both outputs. Cell traces are overlapped for visualization purposes
581 and axis rotated accordingly to show dimensions. **C.** Parameter estimation for cell movement.
582 Different features are included, sequentially, in order to get the final moving procedure for *in*
583 *silico* simulations. Starting from inaccurate movement (C.1) we add size variability due to
584 pressure (C.2), random angles after division (C.3), irregular motion changes (C.4) and slight cell
585 attraction to simulate viscous bodies (C.5). All simulations start from a single cell, and one
586 lineage is colored to monitor coordinate positions. **D.** Synchrony of cell growth. The length of
587 each cell (y axis) is monitored over time (x axis) in both scenarios (experiment, up; simulation,
588 bottom). The initial cells grow at the same time until division point is reached, whereas the third
589 generation of cells grow asynchronously.

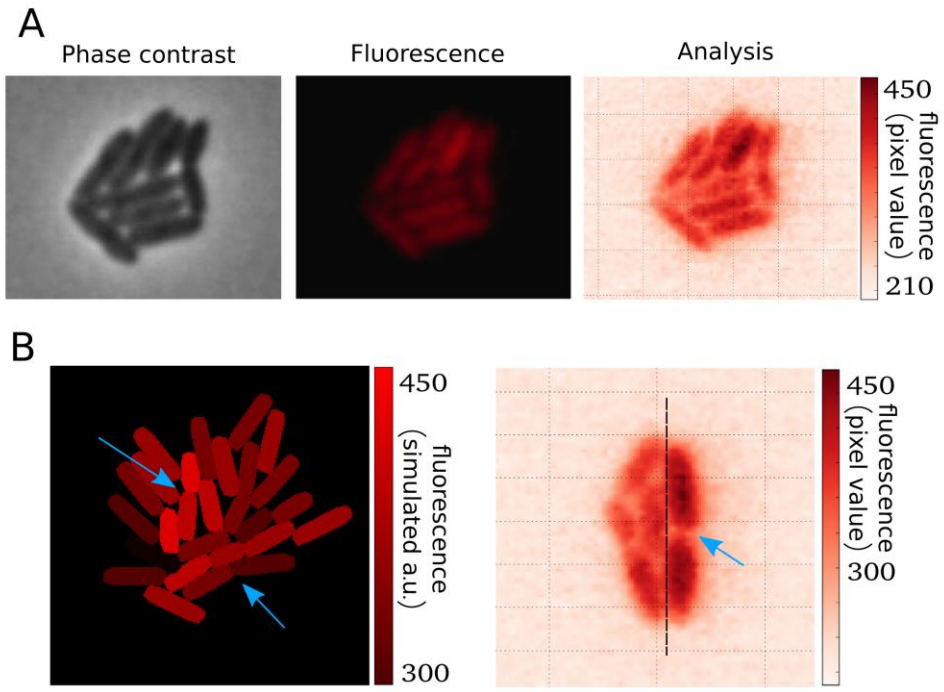

590

591

592 Figure 6: **Spatial progress of the genetic device. A.** Phase contrast image of population (left),
593 fluorescent picture (middle) and computational analysis (right). In the latter, the color scheme
594 (right bar) represents the value of the red channel of every pixel from 0 to 255. However it is
595 transformed into a [0,450] scale in order to allow comparisons with previous fluorescence
596 measurements. **B.** On the left, a simulation of a colony starting from a single cell is shown.
597 Upper-left arrow highlights cells with slower growth rate and RFP accumulation while bottom-
598 right arrow points at a recently divided cell where both daughters share similar RFP
599 concentration. On the right, expression noise inheritance is indicated with an arrow. Furthermore,
600 RFP accumulation caused by slow growth can be observed by the black line separation: a single
601 cell started from each side.